Simulation of permafrost and seasonally frozen ground conditions on the Tibetan Plateau, 1981–2010

Donglin Guo[1,2] and Huijun Wang[1,3]

Received 20 November 2012; revised 12 March 2013; accepted 1 May 2013; published 7 June 2013.

[1] Permafrost and seasonally frozen ground conditions on the Tibetan Plateau were investigated using the Community Land Model, version 4 (CLM4), forced by a suite of new, high-resolution data. This new data set was highly accurate and had an advantage in the frozen ground simulations for its fine temporal and spatial resolution. The simulated current (1981–2000) near-surface permafrost area was 151.50×10^4 km^2, which is close to, but slightly larger than, the range from previous studies ($111.80 \sim 150.0 \times 10^4$ km^2). The simulated current active layer thicknesses ranged from 0 to 4.74 m, with an average of 2.01 m. The other frozen ground parameters, such as the maximum freezing depths for seasonally frozen ground, the date of freeze start, the date of freeze end, and the freeze duration at 1 m depth, were also examined. Considering the issue of scale mismatch, the simulated soil temperature and other frozen ground parameters were reasonable compared to our observations. In response to the Plateau warming of approximately 0.44°C/decade from 1981 to 2010, the near-surface permafrost area decreased at a rate of 9.20×10^4 km^2/decade, and the area-mean active layer thickness increased by 0.15 m/decade. The area-mean maximum freezing depth of the seasonally frozen ground decreased by 0.34 m/decade. At a depth of 1 m, the dates of freeze start for permafrost and seasonally frozen ground delayed linearly by 3.8 and 4.0 days/decade, respectively, while the dates of freeze end for them advanced linearly by 5.9 and 4.6 days/decade, respectively. These trends in the dates of freeze start and freeze end resulted in freeze durations that were shortened by 9.7 and 8.6 days/decade for permafrost and seasonally frozen ground, respectively. These results give detailed permafrost and seasonally frozen ground states as well as their changes, which will be useful for studying frozen ground's response to climate change and frozen ground engineering stabilization.

Citation: Guo, D., and H. Wang (2013), Simulation of permafrost and seasonally frozen ground conditions on the Tibetan Plateau, 1981–2010, *J. Geophys. Res. Atmos.*, *118*, 5216–5230, doi:10.1002/jgrd.50457.

1. Introduction

[2] With an average elevation of more than 4000 m, the Tibetan Plateau is the highest and the most extensive plateau in the world [*Liu and Chen*, 2000]. Almost all of the Tibetan Plateau is underlain by permafrost and seasonally frozen ground because of its high elevation. The present permafrost on the Tibetan Plateau is a relict of the late Pleistocene permafrost, which had degraded during the Holocene [*Jin et al.*, 2007]. It has higher temperature and thus being particularly susceptible to climate change [*Qiu and Cheng*, 1995; *Jin et al.*, 2007]. A significant climate warming has occurred on the Tibetan Plateau during the recent decades [*Liu and Chen*, 2000; *Guo and Wang*, 2011]. This warming will necessarily result in thawing of permafrost on the Tibetan Plateau. Previous studies indicated that permafrost thawing can affect local hydrology, ecosystems, soil biogeochemistry, and engineering infrastructure [*Nelson et al.*, 2001; *Nelson*, 2003; *Lawrence and Slater*, 2005; *Zimov et al.*, 2006; *Schuur et al.*, 2009; *Guo et al.*, 2012]. Therefore, detailed investigation of permafrost change on the Tibetan Plateau is of great importance in understanding the Plateau's ecological environment change as well as guiding the construction and maintenance of human infrastructures (such as Qinghai-Tibet railway).

[3] Some observational studies have been conducted on the Tibetan Plateau in recent years [*Wang et al.*, 2000; *Cheng and Wu*, 2007; *Wu and Zhang*, 2008, 2010; *Yang et al.*, 2010]. These observational studies provide some important facts, but they are restricted in representation due to the sparse number of field observational sites on the Tibetan Plateau. Studies focusing on the Plateau's frozen ground at the regional scale and long-term time scales are quite useful but currently still few. Numerical simulation can be an appropriate method for expanding a site study to the regional and long-term time scales, but this method is

[1]Nansen-Zhu International Research Center (NZC), Institute of Atmospheric Physics, Chinese Academy of Sciences, Beijing, China.
[2]Graduate University of Chinese Academy of Sciences, Beijing, China.
[3]Climate Change Research Center, Chinese Academy of Sciences, Beijing, China.

Corresponding author: D. Guo, Nansen-Zhu International Research Center (NZC), Institute of Atmospheric Physics, Chinese Academy of Sciences, PO Box 9804, Beijing 100029, China. (guodl@mail.iap.ac.cn)

2169-897X/13/10.1002/jgrd.50457

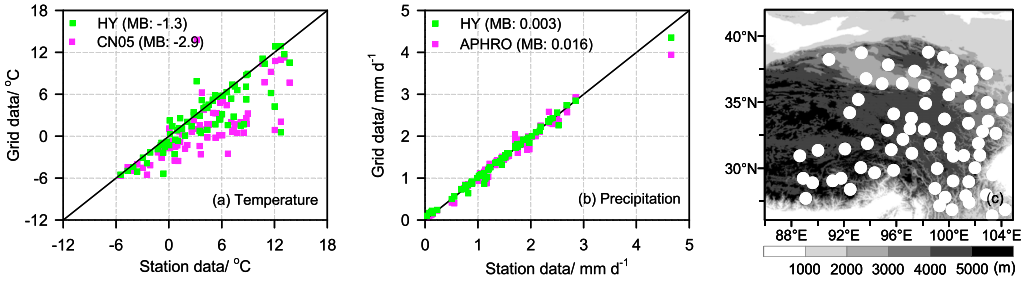

Figure 1. Comparison of the (a) gridded HY and CN05 air temperatures as well as the (b) gridded HY and APHRO precipitation with the (c) corresponding station observations from 72 meteorological stations located in the Tibetan Plateau. MB denotes the mean bias.

usually difficult for the Tibetan Plateau because the Plateau's rugged and varied topographic characteristics require high-resolution forcing data and a sophisticated frozen ground model. Development of scientific researches has brought opportunities [*Ju et al*., 2007; *He*, 2010; *Lawrence et al*., 2011; *Gao et al*., 2012]. *Guo et al*. [2012] projected the Plateau's permafrost degradation during the 21st century and the impact of permafrost degradation on local hydrological processes using the Community Land Model, version 4 (CLM4), forced by archived data (every 6 h and $0.2^\circ \times 0.2^\circ$ in longitude and latitude) from RegCM3 (Regional Climate Model version 3) nested within the MIROC3.2 HiRes (Model for Interdisciplinary Research on Climate 3.2 hires).

[4] The objectives of this study are (1) use a suite of new, high-resolution (every 3 h and $0.1^\circ \times 0.1^\circ$ in longitude and latitude) atmospheric data to force CLM4 to investigate in more detail the Plateau's permafrost and seasonally frozen ground and their changes during the recent decades, (2) validate the simulated results with in situ observations, and (3) examine the Plateau's soil freeze/thaw cycle at 1 m depth and its change during the recent decades.

2. Data, Model, Experimental Design, and Methods

2.1. Data

[5] The monthly surface air temperature and precipitation for 72 meteorological stations above 2000 m that were used for forcing data evaluation were obtained from the Data and Information Center, China Meteorological Administration. The data cover the period from 1961 to 2007. The stations have an uneven distribution, and majority of the stations are situated in the eastern and central Tibetan Plateau (Figure 1c). The data have carried out basic logic and spatial consistency tests and thus are reliable. These data have been widely used in research on climate change over the Tibetan Plateau [*Sun et al*., 2010; *Guo and Wang*, 2011; *Wang and Zeng*, 2012].

[6] The daily temperature grid data that were used for forcing data evaluation were derived from the China Meteorological Administration (CN05). These grid data have a resolution of $0.5^\circ \times 0.5^\circ$ in longitude and latitude and cover the period from 1961 to 2009. These data were developed by interpolating 751 stations observations in China [*Xu et al*., 2009] and have been widely used for validation of model's performance [*Gao et al*., 2012; *Guo et al*., 2012].

[7] The precipitation grid data used for forcing data evaluation were developed by the Asian Precipitation-Highly Resolved Observational Data Integration Towards Evaluation of the Water Resources Project in collaboration with the Research Institute for Humanity and Nature and the Meteorological Research Institute of the Japan Meteorological Agency (APHRO). This data set has a resolution of 0.25° 0.25° in longitude and latitude and covers the period from 1951 to 2007. The data were constructed by interpolating rain gauge observations obtained from meteorological and hydrological stations throughout the region. More detailed information is provided by *Yatagai et al*. [2009].

Table 1. Information of Site Observations at a Depth of 1 m

Station Name	Latitude (deg)	Longitude (deg)	Elevation (m)	Observation Period	Type of Frozen Ground
KM1	35.63	94.07	4770	1996–2002	Permafrost
KM2	35.62	94.07	4759	1996–2002	Permafrost
D66	35.52	93.78	4560	1997–2007, missing period: Oct 1999 to Aug 2000, Jan to Aug 2006	Permafrost
CM1	35.51	93.74	4552	1996–2001	Permafrost
CM2	35.40	93.53	4482	1996–2006	Permafrost
WD1	35.23	93.09	4610	1996–2001	Permafrost
WD2	35.13	93.04	4707	1996–2006	Permafrost
D105	33.06	92.16	5020	1998–2005	Permafrost
TG1	32.71	91.87	4997	1999–2006	Permafrost
D110	32.69	91.86	5000	1998–1999, 2003–2005	Permafrost
TM1	32.49	91.82	4873	1999–2006	Permafrost
AD1	32.38	91.71	4786	1999–2006	Permafrost
Anduo	32.24	91.62	4710	1998–2002, 2005	
BJ	31.37	91.90	4509	2001–2007	Seasonally frozen ground
MS3608	31.23	91.78	4610	1997–2009, missing period: Sep 2001 to Aug 2002, Mar to Aug 2006	Seasonally frozen ground

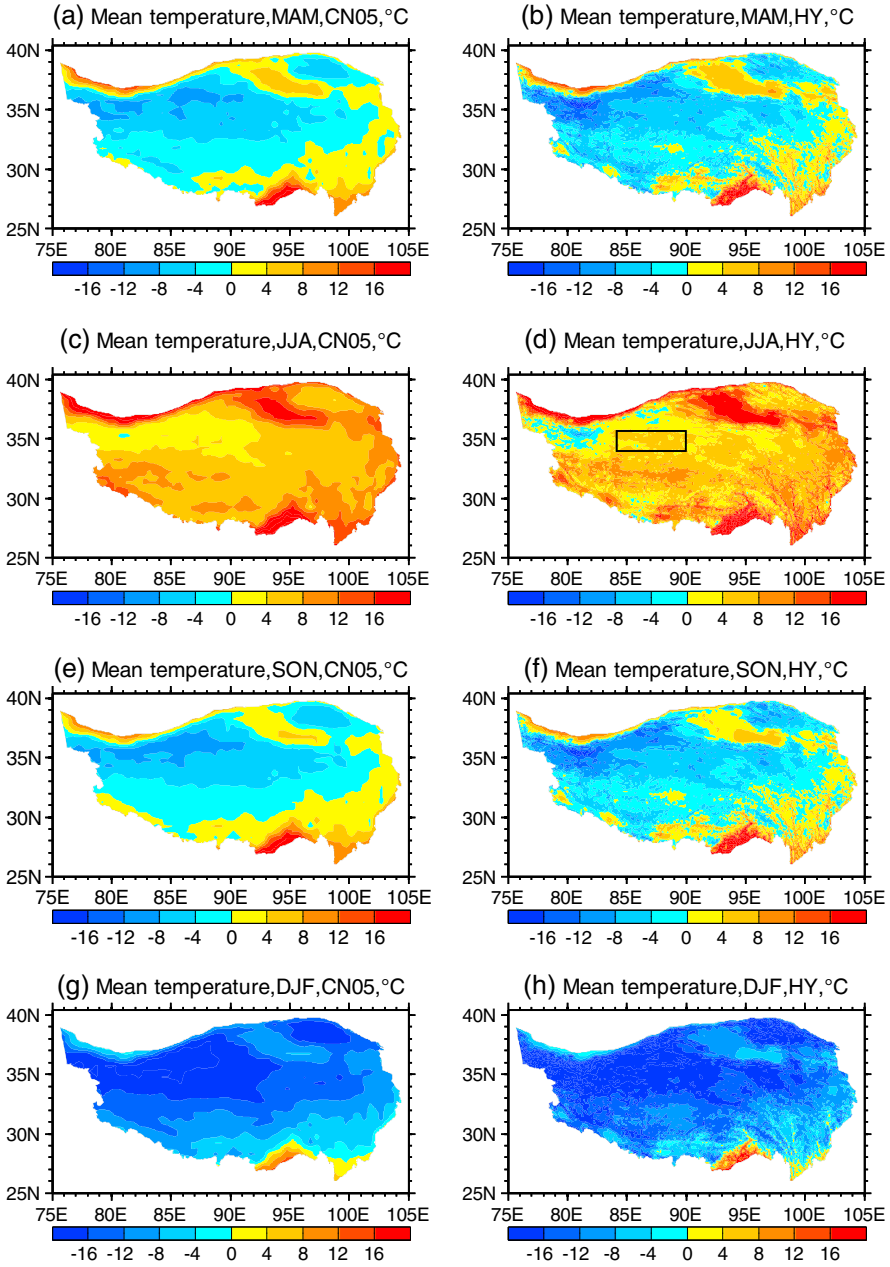

Figure 2. Comparison of the mean HY with CN05 air temperature, averaged over 1981 to 2000. (a and b) Spring (MAM), (c and d) summer (JJA), (e and f) autumn (SON), and (g and h) winter (DJF). The rectangle in subgraph (Figure 2d) is for comparison with that in Figure 8a.

[8] The atmospheric forcing data that were used in this work were developed by the Hydrometeorological Research Group at the Institute of Tibetan Plateau Research, Chinese Academy of Sciences [*He*, 2010] (HY data). The temporal and spatial resolutions of the preliminary version of this data set were every 3 h and $0.25^\circ \times 0.25^\circ$ in longitude and latitude from 1998 to 2006. After several updates, the latest version was released in May 2012 and has a temporal and spatial resolution of every 3 h and $0.1^\circ \times 0.1^\circ$ in longitude and latitude from 1981 to 2010, covering the entire region of China. The near-surface air temperature, pressure, wind speed, and specific humidity were constructed by merging 740 meteorological stations' observations with corresponding Princeton meteorological forcing data [*Sheffield et al.*, 2006]. The observation height for air temperature and specific humidity was 1.5 m above the ground, while wind speed was measured 10 m above the ground. The precipitation data set was constructed by combining three precipitation data sets, including observations from 740 meteorological stations, the Tropical Rainfall Measuring Mission (TRMM) 3B42 precipitation products [*Huffman et al.*, 2007], and the Asian Precipitation-Highly Resolved Observational Data Integration Towards Evaluation of the Water Resources project [*Yatagai et al.*, 2009]. The downward shortwave radiation was obtained by correcting the Global Energy and Water Cycle Experiment-Surface Radiation Budget shortwave radiation data set [*Pinker and Laszlo*, 1992], with reference to radiation estimates from

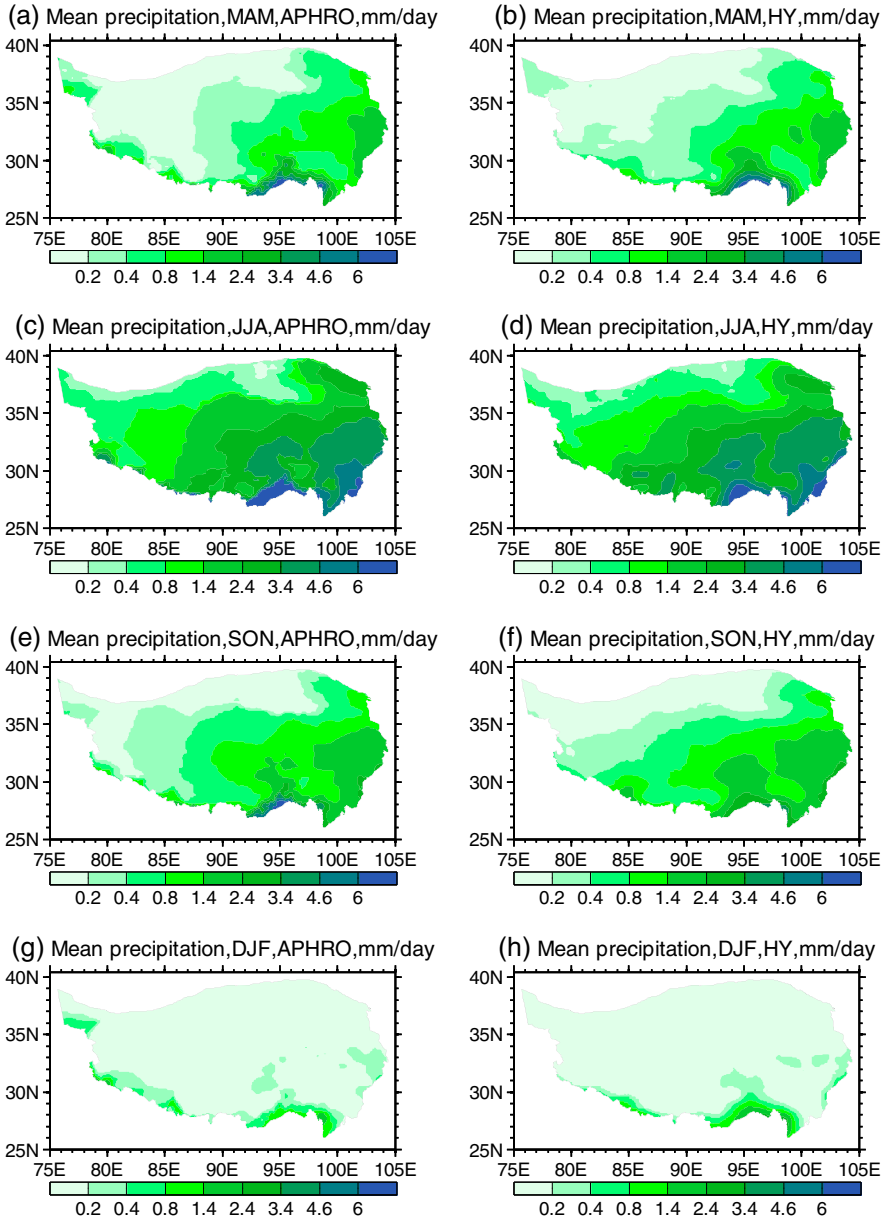

Figure 3. Comparison of the mean HY with APHRO precipitation, averaged over 1981 to 2000. (a and b) Spring (MAM), (c and d) summer (JJA), (e and f) autumn (SON), and (g and h) winter (DJF).

meteorological station data using a hybrid radiation model [*Yang et al.*, 2006]. The downward longwave radiation was estimated using *Crawford and Duchon*'s [1999] model, which is driven by the known near-surface air temperature, pressure, specific humidity, and downward shortwave radiation. This data set is available at the following Web site: http://westdc.westgis.ac.cn/data/7a35329c-c53f-4267-aa07-e0037d913a21.

[9] *He* [2010] presented an evaluation of this forcing data set compared to site observations from the Global Energy and Water Cycle Experiment/Asian Monsoon Experiment (GAME-Tibet) and the Coordinated Enhanced Observing Period/Asia-Australia Monsoon Project on the Tibetan Plateau (CAMP-Tibet). For three-hourly downward shortwave radiation at 11 sites, the mean bias and the correlation coefficient of them were $-1.60\,\mathrm{W\,m^{-2}}$ and 0.93, respectively. For three-hourly air temperature at four sites, their mean biases and correlation coefficients were $-0.18^{\circ}\mathrm{C}$ and 0.95, respectively. These results indicated that the constructed forcing data set was reliable. Subsequently, *Chen et al.* [2011] found that the mean land surface temperature bias in early afternoon could be reduced by more than $2^{\circ}\mathrm{C}$ when this new forcing data set was used to drive the Noah model.

[10] The majority of soil temperature and active layer thickness observations that were used to validate the simulated results were derived from *Wu and Zhang* [2008, 2010]. The other soil temperature observations were obtained from the GAME-Tibet and the CAMP-Tibet. The information from the observations is presented in Table 1. Detailed observational information is described in *Yang et al.* [2003] and *Guo et al.* [2011a, 2011b].

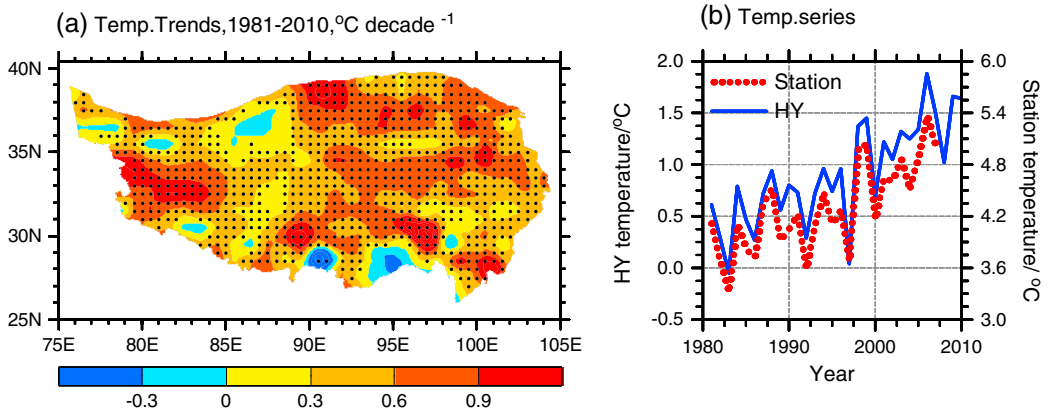

Figure 4. (a) Spatial distribution of trends in the air temperature of the HY forcing data from 1981 to 2010 and the (b) comparison of the annual air temperature time series from the HY data as averaged over the entire Tibetan Plateau with that from 72 meteorological stations. Areas with significance level exceeding 95% are denoted with dots.

[11] The Plateau's frozen ground map, used to validate the simulated frozen ground distributions, was developed by *Li and Cheng* [1996]. This map is currently thought to present a reasonable distribution pattern of frozen ground on the Tibetan Plateau [*Zhao*, 2004; *Cheng and Wu*, 2007; *Ran et al*., 2012]. However, the map may still be inaccurate in some areas because it was produced based on sparse borehole observations and terrain data [*Li and Cheng*, 1996].

2.2. Model

[12] The land-surface model CLM4 was used in this study [*Oleson et al*., 2010]. It is the latest version of CLM model, from the update of the CLM3.5. *Guo et al*. [2012] provide a more detailed description of the features and improvements of CLM4. The modifications that are directly relevant to this study include an explicit treatment of the frozen ground processes, an incorporation of a freezing point depression expression, a representation of the thermal and hydraulic properties of soil organic matter, and a deepening of the soil column (approximately 50 m). It has been well demonstrated that these modifications are able to greatly improve the accuracy of frozen ground simulations [*Burn and Nelson*, 2006; *Lawrence and Slater*, 2006; *Niu and Yang*, 2006; *Yi et al*., 2007; *Delisle*, 2007; *Nicolsky et al*., 2007; *Alexeev et al*., 2007; *Lawrence and Slater*, 2008; *Lawrence et al*., 2011]. Hence, the use of CLM4 was advantageous for the simulation of frozen ground.

2.3. Experimental Design

[13] Six atmospheric forcing elements are required by CLM4, including incoming shortwave radiation flux, precipitation, wind speed, air temperature, specific humidity, and atmospheric pressure. The HY data (every 3 h and $0.1^\circ \times 0.1^\circ$ in longitude and latitude) were used as atmospheric forcing data. A regional simulation was performed, and CLM_QIAN was selected as the DATM (Data Atmosphere) mode. The model domain is 20°N to 45°N and 70°E to 105°E. The simulation yielded daily output results with a spatial resolution of $0.31^\circ \times 0.23^\circ$ in longitude and latitude. The simulations were spun up for 400 years with the RegCM3's results from 1951 [*Gao et al*., 2012] and for continuous 100 years with HY data from 1981. The change in soil temperature was less than 0.001°C/year at all soil levels when the spin-up phase ended. The period of simulation was from January 1981 to December 2010.

2.4. Methods

[14] In the soil layers of the upper 4.7 m soil of a model grid cell, if there is at least one layer in which the monthly soil temperature remains below 0°C for 24 consecutive months, we identify this grid cell as containing near-surface permafrost. Similarly, in the soil layers of the upper 4.7 m soil of a model grid cell, if there is no layer in which the monthly soil temperature remains below 0°C for 24 consecutive months but there is at least one layer in which the monthly soil temperature remains below 0°C for a period of 24 consecutive months, we identify this grid cell as containing seasonally frozen ground. The annual active layer thickness was defined as the maximum thawing depth during the period from January 1 to December 31, which was calculated by daily data. Before the active layer thickness was calculated, the soil temperature layers first were linearly interpolated to evenly spaced layers with a thickness of 0.01 m. To avoid the potential impact of random soil temperature on the movement from one soil phase to the next when calculating the dates of freeze start and freeze end, the passage of three consecutive days meeting a chosen category of criteria (i.e., daily soil temperature below or above zero)

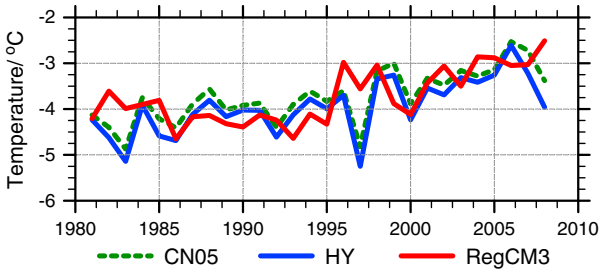

Figure 5. Comparison of the area-mean time series of air temperature between HY, RegCM3, and CN05 data from 1981 to 2010, averaged over the area 30°N to 36°N; 83°E to 100°E.

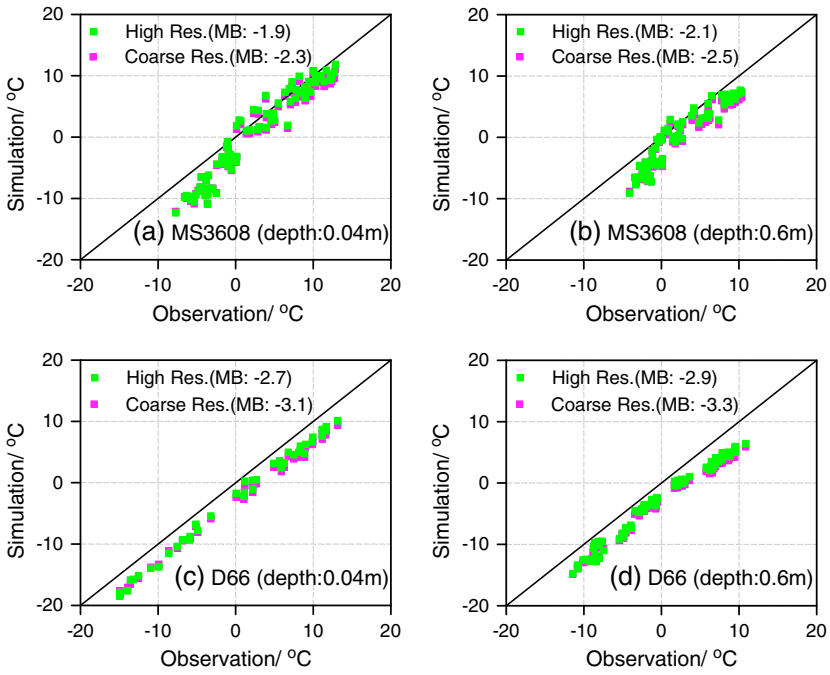

Figure 6. Comparison of monthly gridded soil temperature from the simulation driven by high resolution (every 3 h, $0.1^\circ \times 0.1^\circ$ in longitude and latitude) and coarse resolution (every 6 h, $0.2^\circ \times 0.2^\circ$ in longitude and latitude) forcing data, with the corresponding site observations at (a, c) 0.04 m and (b, d) 0.6 m depth at the MS3608 and D66 sites from 1998 to 2006. MB denotes the mean bias.

was used as the indicator of the phase change, and the first day of these three days was recorded as the start date of the next phase. The change rate of the frozen ground parameters was calculated using ordinary least squares regression by deriving the slope of the linear fit. The significance of the trends was assessed using a nonparametric test approach [*Wang and Swail*, 2001; *Wei*, 2007].

3. Results

3.1. Evaluation of the Forcing Data

[15] The quality of the simulation of frozen ground was largely dependent on the accuracy of the atmospheric forcing data [e.g., *Wang and Zeng*, 2011; *Lawrence et al.*, 2012]. Thus, we evaluated the data before the simulation. Specifically, we compared them with CN05 data and APHRO data, respectively, to evaluate spatial patterns. To evaluate the magnitude, we compared the data with meteorological station observations. The spatial distribution pattern of HY air temperature was similar to that of the CN05 data in the spring, autumn, and winter, their spatial correlation coefficients were 0.87, 0.87, and 0.90 for these three seasons, respectively. Clearly, the HY air temperature includes more detailed information due to its high spatial resolution (Figure 2). In summer, the spatial distribution pattern of HY air temperature is also similar to that of CN05 (spatial correlation coefficient is 0.83), except that the HY air temperature is higher than the CN05 data in the northwestern region of the Plateau (i.e., the area that is surrounded by the blue rectangle in Figure 2d). In this area, we could not determine which data (CN05 or HY) were more accurate because there were no station observations there. Further observational studies are required to rectify this situation in the future. However, compared to the 72 meteorological stations' observations from the central and eastern regions of the Plateau, the HY air temperature had a mean bias of -1.30°C, which was much smaller than the mean bias of -2.90°C for the CN05 air temperature (Figure 1a). The higher resolution of the HY data could represent more detailed topography information, which favors the smaller bias in air temperature.

[16] For precipitation, the spatial distribution pattern of the HY data was quite close to that of the APHRO data in all four seasons, and their spatial correlation coefficients were 0.95, 0.86, 0.91, and 0.80 for the spring, summer, autumn, and winter, respectively (Figure 3). Similarly, compared to the 72 meteorological stations' data, the HY precipitation had a mean bias of 0.003 mm/d, which was also much smaller than the mean bias of 0.016 mm/d in the APHRO precipitation data (Figure 1b).

[17] The time series of the HY temperature data was also compared to those of the 72 meteorological stations (Figure 4b) and the CN05 data (Figure 5). The interannual changes of the HY and the observed temperature data were very consistent, with a correlation coefficient of 0.95; however, their magnitudes were different because the meteorological station observations cover the eastern and central Plateau, while the HY temperature covers the entire Plateau. In addition, the rate of increase in the HY air temperature was 0.44°C/decade, which is similar to the 0.48°C/decade rate of increase at the 72 meteorological stations from 1981 to 2007. The time series of HY air temperature was also quite consistent with that of the CN05 air temperature in the chosen area of 30°N to 36°N and 83°E to 100°E. Their increasing rates of air temperature were 0.49 and 0.52 °C/decade, respectively. These results indicate that the

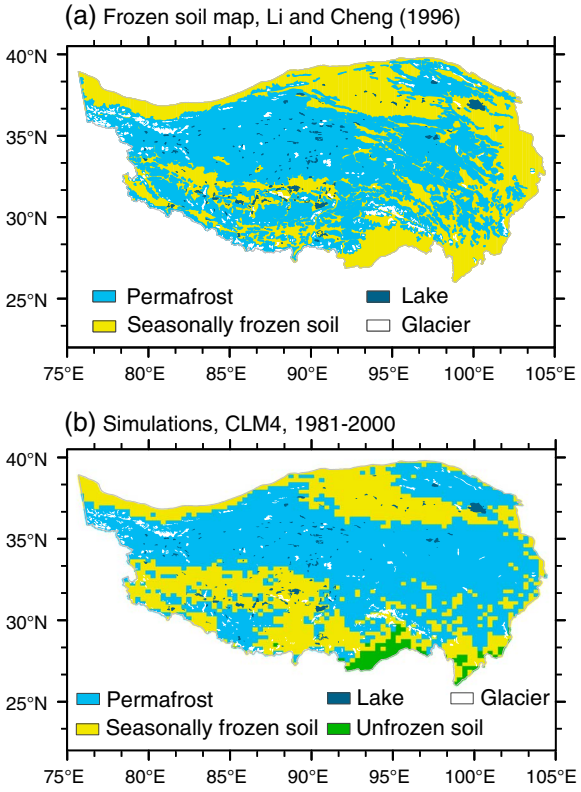

Figure 7. Comparison of the simulated results with the Plateau's frozen ground map. (a) The Plateau's frozen ground map (after the work by *Li and Cheng* [1996]) and (b) the simulated mean distribution pattern of permafrost and seasonally frozen ground from 1981 to 2000.

HY data were high quality and suitable for the frozen ground simulation of the Tibetan Plateau.

[18] To further explore the impact of the temporal and spatial resolution of the atmospheric forcing data on the frozen ground simulation, we performed two simulations that were driven by the HY forcing data, one with higher resolution (every 3 h and $0.1^\circ \times 0.1^\circ$ in longitude and latitude) and one with coarser resolution (every 6 h and $0.2^\circ \times 0.2^\circ$ in longitude and latitude). The coarser-resolution forcing data were derived by interpolating the higher-resolution forcing data. The results indicated that soil temperatures from the simulation that was driven by the higher resolution forcing data were closer to the observations than those from the simulation that was driven by the coarser resolution forcing data (Figure 6). The mean bias between the simulated and observed soil temperatures was reduced by 0.40°C at sites D66 and MS3608 when the simulation was driven using the higher-resolution forcing data. This result implies that the higher-resolution atmospheric forcing data are useful for improving the accuracy of the frozen ground simulation, at least at this level of resolution. Therefore, the use of higher-resolution atmospheric forcing data was advantageous to our study.

3.2. Frozen Ground Simulation and Validation

3.2.1. Frozen Ground Simulation

[19] As shown in Figure 7, the simulated permafrost and seasonally frozen ground distributions were very similar to the Plateau's frozen ground map. Compared to the results from *Guo et al.* [2012], this study produced a more detailed frozen ground distribution because of its use of the new atmospheric forcing data. However, more permafrost was simulated in the eastern region of the Plateau and less permafrost was simulated in the southwestern region of the Plateau. The discrepancies between the simulated results and the Plateau's frozen ground map could be partially attributed to possible inaccuracies in the soil organic matter content and the soil texture data in the model. In addition, the discrepancies could also be due to possible inaccuracies in the Plateau's frozen ground map.

[20] The simulated permafrost covered a total area of 151.50×10^4 km^2 (excluding glaciers and lakes). This area was similar to, but slightly larger than, the range of $111.80 \sim 150.0 \times 10^4$ km^2 from previous studies (Table 2). The model also yielded a total seasonally frozen ground area of 87.10×10^4 km^2 (excluding glaciers and lakes) and a total unfrozen ground area of 6.10×10^4 km^2 (Table 2).

[21] The simulated mean active layer thickness from 1981 to 2000 is displayed in Figure 8a. The simulated active layer thickness was shallowest in the northwestern corner of the permafrost area, with a range of approximately 0–2 m. It was also relatively shallow in some grids in the eastern permafrost area, with a range of approximately 1–2 m. Evidently, the active layer thickness in the black rectangle was relatively deep, with a range of approximately 2–3 m. This was related to the relatively higher summer air temperature in this region, as depicted in Figure 2d. For the whole permafrost area, the active layer thickness ranged from 0 to 4.74 m, with an average of 2.01 m.

[22] The spatial distribution patterns of the simulated date of freeze start, date of freeze end, and freeze duration at a depth of 1 m were similar to that of the active layer thickness (Figures 8b–8d). Basically, the permafrost with shallower active layer thickness, e.g., in the northwestern corner of the permafrost area, had an earlier date of freeze start, a later date of freeze end, and a longer freeze duration, while the

Table 2. Total Area of Frozen Ground on the Tibetan Plateau, as Calculated Using Different Methods (Unit: 10^4 km^2)

Methods	Permafrost Area	Seasonally Frozen Ground Area	Unfrozen Ground Area	Data Sources
Regional statistical survey	150.0			*Zhou and Guo* [1983]
Historical data analysis	140.10			*Li and Cheng* [1996]
Altitude model	129.40			*Li and Cheng* [1999]
Digitized map	126.70	122.40		*Nan* [2003]
Altitude model	136.0			*Nan* [2003]
The surface frost number	127.80	123.60		*Nan* [2003]
Mean annual ground temperature model	111.80			*Nan* [2003]
TTOP (Temperature at the Top of Permafrost) model	138.70			*Nan* [2003]
RegCM3/CLM4	122.20	127.90	1.20	1980–2000 average, *Guo et al.* [2012]
HY/CLM4	151.50	87.10	6.10	1981–2000 average, this study

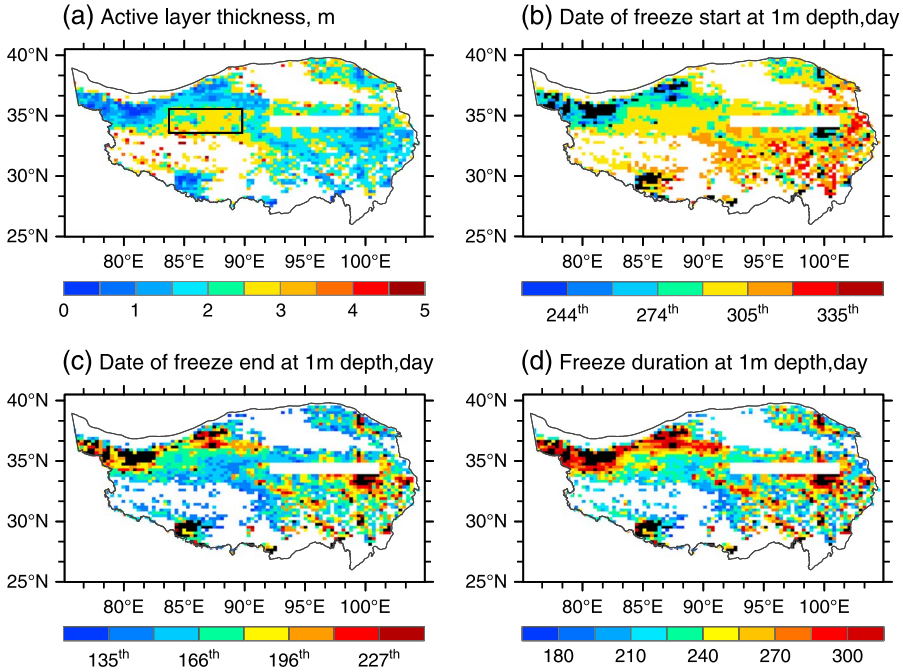

Figure 8. Spatial distribution of the (a) simulated active layer thickness, (b) date of freeze start at 1 m depth, (c) date of freeze end at 1 m depth, and (d) freeze duration at 1 m depth of permafrost, averaged over 1981 to 2000. Black grids represent those areas where soil does not thaw to 1 m depth over the course of the year. Data in the belt (near 34.10°N to 35.04°N; 92.19°E to 100.93°E) were removed because the simulated results in this belt could be inaccurate. This is related to the possible inaccuracy of the soil organic matter content in these locations because the global organic matter data used in the model are based on relatively few observations [*Guo et al.*, 2012].

permafrost with the deeper active layer thickness, e.g., in the black rectangle on Figure 8a, had a later date of freeze start, an earlier date of freeze end, and a shorter freeze duration. The area-averaged dates of freeze start, date of freeze end, and freeze duration at a depth of 1 m were approximately the 296th day (23 October), the 174th day (23 June), and 254 days, respectively (Table 3).

[23] The simulated current maximum freezing depth, date of freeze start, date of freeze end, and freeze duration at a depth of 1 m for seasonally frozen ground are presented in Figure 9. The maximum freezing depth was relatively shallow in the grids located in the center of the seasonally frozen ground area but was relatively deep in the grids located at the edge of the seasonally frozen ground area. Despite these features of distribution, the shallowest maximum freezing depth was located in the southern region of the seasonal frozen ground area. For the whole seasonally frozen ground area, the area-mean for maximum freezing depth was 2.47 m.

[24] The spatial distribution patterns of the simulated date of freeze start, date of freeze end, and freeze duration at a depth of 1 m were similar to those of the maximum freezing depth. Basically, seasonally frozen ground with shallower maximum freezing depth, e.g., in the southern region of the seasonally frozen ground area, had a later date of freeze start, an earlier date of freeze end, and a shorter freeze duration, while seasonally frozen ground with deeper maximum freezing depth, e.g., at the edge of the seasonally frozen ground area, had an earlier date of freeze start, a later date of freeze end, and a longer freeze duration. The area-averaged dates of freeze start, date of freeze end, and freeze duration at a depth of 1 m were approximately the 342nd day (8 December), the 112th day (22 April), and 124 days, respectively (Table 3).

3.2.2. Validation of the Simulated Results With In Situ Observations

[25] Soil temperature was one of the key variables in the evaluation of the frozen ground simulation. For the evaluation of temporal change, we compared the simulated monthly

Table 3. Simulated Values of Various Frozen Ground Parameters, Averaged Over Their Own Areas, as Shown in Figures 8, 9, 11, and 12

	Current (1981–2000)		Changes in 1981–2010 (Per Decade)	
Frozen Ground Parameters	Permafrost	Seasonally Frozen Ground	Permafrost	Seasonally Frozen Ground
Active layer thickness (m)	2.01		0.15	
The maximum freezing depth (m)		2.47		−0.34
Date of freeze start at 1 m depth (day)	296th	342nd	3.8	4.0
Date of freeze end at 1 m depth (day)	174th	112th	−5.9	−4.6
Freeze duration at 1 m depth (days)	254	124	−9.7	−8.6

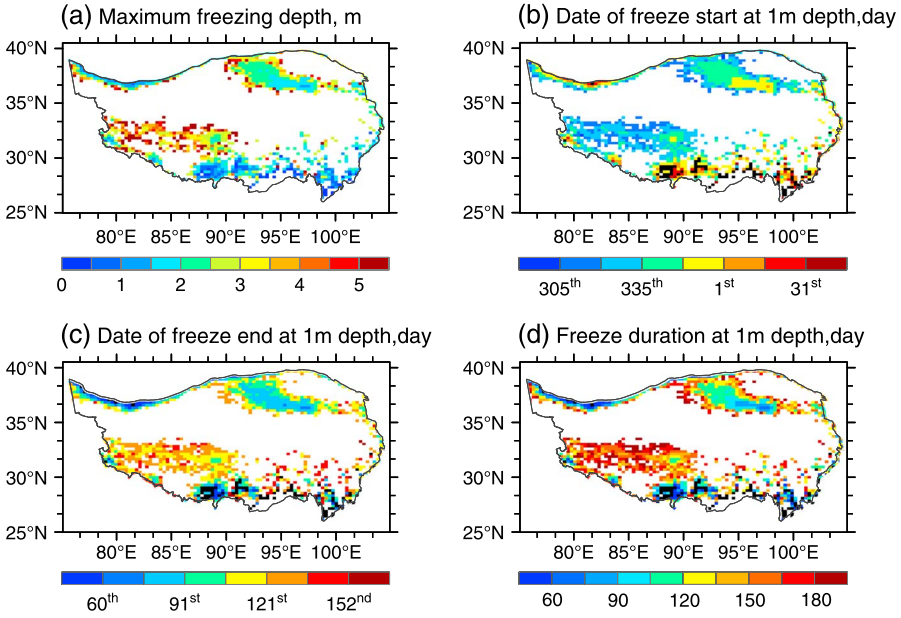

Figure 9. Spatial distribution of (a) simulated maximum freezing depth, (b) date of freeze start at 1 m depth, (c) date of freeze end at 1 m depth, and (d) freeze duration at 1 m depth of seasonally frozen ground, averaged over 1981 to 2000. Black grids represent those areas where soil does not freeze to 1 m depth over the course of the year.

gridded soil temperatures with the corresponding site observations (i.e., the grids containing measured sites) at depths of 0.04 m and 0.6 m at sites D66 and MS3608 from 1998 to 2006 (Figure 6). Notably, the model did not directly calculate the soil temperatures at depths of 0.04 m, 0.6 m, 1 m, or 6 m. Soil temperatures at these layers were estimated using simple linear interpolation between the known values. As displayed in Figures 6a and 6b, the simulated monthly gridded soil temperatures showed good agreement with the corresponding observations at site MS3608. Their mean biases were −1.90°C and −2.10°C, and their correlation coefficients were 0.97 and 0.94 at depths of 0.04 m and 0.6 m, respectively. At site D66, the simulated monthly gridded soil temperatures were close to, but systematically lower than, the corresponding observations, with mean biases of −2.70°C and −2.90°C and correlation coefficients of 1.00 and 0.99 at depths of 0.04 m and 0.6 m, respectively (Figures 6c and 6d).

[26] For the evaluation of spatial change, we compared the simulated gridded mean soil temperatures at 1 m and 6 m depths, the active layer thickness, the maximum freezing depth, the date of freeze start, the date of freeze end, and the freeze duration with the corresponding observations at 15 sites (Figure 10). Among all 15 sites, the mean bias between the simulated soil temperatures and the corresponding site observations at a depth of 1 m ranged from −0.20 to −3.20°C, with a mean of −1.80°C (Figure 10a). At a depth of 6 m, the mean bias between the simulated soil temperatures and the corresponding site observations ranged from −0.10 to −2.50°C, with a mean of −1.30°C for all nine sites (Figure 10b).

[27] As displayed in Figure 10c, the simulated active layer thicknesses at five sites were close to the corresponding site observations, with biases of less than 0.40 m. However, at the remaining four sites, the biases were relatively large (0.57 to 1.76 m). Among all nine sites, the mean bias between the simulated active layer thickness and the corresponding site observations was −0.02 m (the mean absolute bias was 0.70 m). There were only two sites with observations for the maximum freezing depth. The simulated maximum freezing depth was evidently shallower than that of the site observations at these two sites, with a mean bias of 1.40 m (Figure 10d).

[28] The simulated date of freeze start at 1 m depth fit best with the corresponding observations at two sites, with biases of less than 10.5 days (Figure 10e). At the remaining four sites, the simulated date of freeze start was −16.5 to −44 days earlier than the corresponding observations. The mean bias for all six sites was −21 days. The simulated date of freeze end at 1 m depth also fit well with the corresponding observations at two sites, with biases of less than 4 days (Figure 10f), but the bias was large at the remaining four sites (−17.8 to 45 days). For all six sites, the mean bias was 12 days. The simulated freeze duration at 1 m depth was longer than the corresponding observations, except for the D110 site. The mean bias between the simulated freeze duration and the corresponding observations for all six sites was 33 days (Figure 10g).

[29] It should be noted that a scale mismatch existed in these comparisons because they were based on grid-mean simulated results and individual site observations. Furthermore, the measured active layer thickness, date of freeze start, date of freeze end, and freeze duration tended to vary substantially over small distances. This could be especially significant on the Tibetan Plateau, where the topography is very rugged and varied. In addition, the observation sites on the Tibetan Plateau were usually located in plains, basins, and valleys at relatively low altitudes where the permafrost may have been relatively warmer than that at adjacent higher altitude areas [*Wu et al.*, 2010]. In this case, the grid containing the observation site and the adjacent higher altitude areas would have a lower grid-mean soil temperature than the observation site. Considering these sampling issues, the simulated frozen ground parameters were basically reasonable.

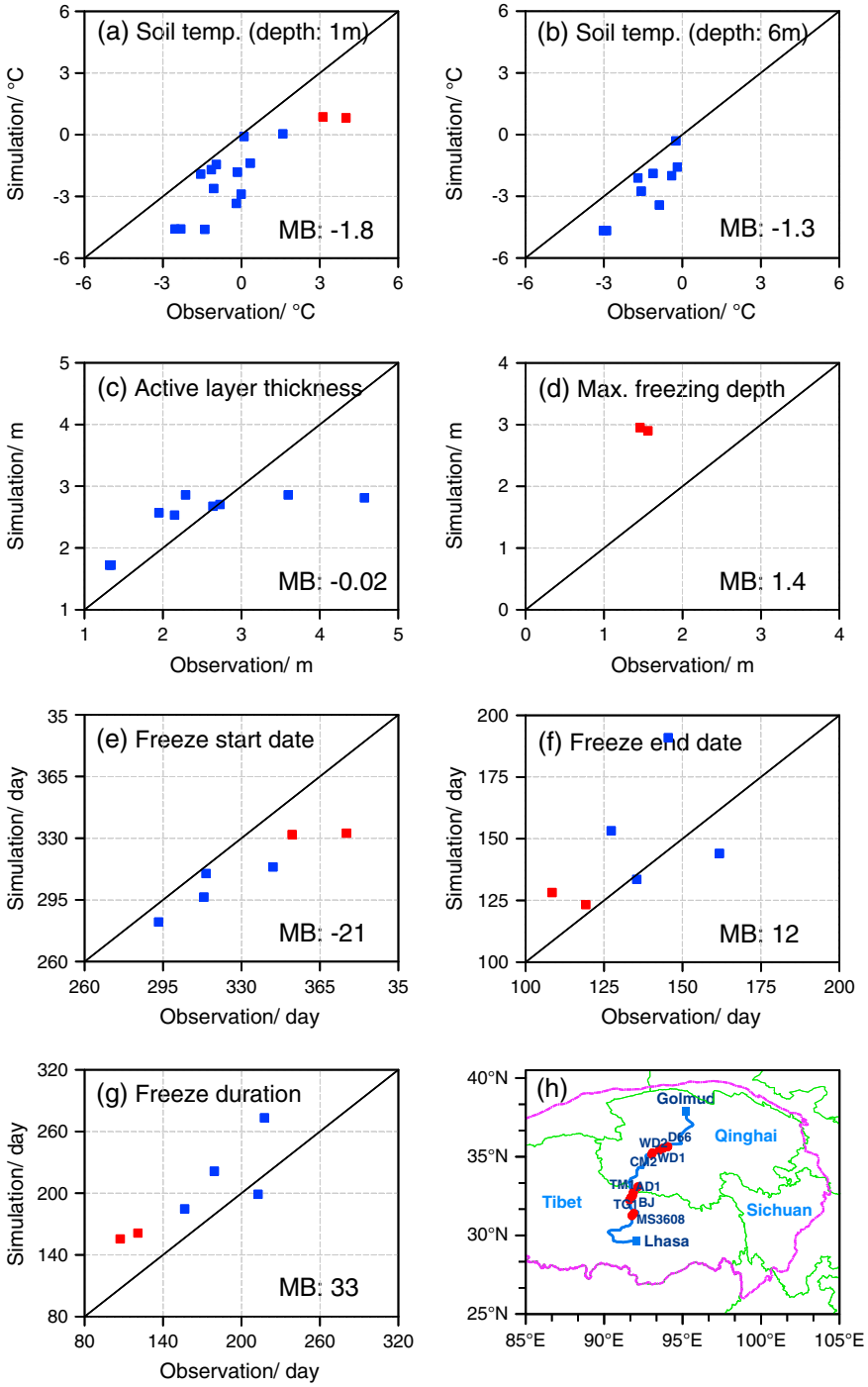

Figure 10. Comparison of the simulated annual-mean gridded soil temperature at (a) 1 m and (b) 6 m depths, (c) active layer thickness, (d) maximum freezing depth, (e) freeze start date at 1 m depth, (f) freeze end date at 1 m depth, and (g) freeze duration at 1 m depth with the corresponding mean site observations, averaged over 1996 to 2006 (for some sites with shorter observation periods, averaged over their recorded period). The red rectangles represent the sites that were located in the seasonally frozen ground area, while the blue rectangles represent the sites that were located in the permafrost area. The locations of the observed sites are shown in subgraph (Figure 10h). MB denotes the mean bias.

3.3. Changes in Frozen Ground During 1981–2010

[30] The spatial pattern of trends in the active layer thickness, the date of freeze start, the date of freeze end, and the freeze duration at a depth of 1 m in permafrost areas from 1981 to 2010 is presented in Figure 11. The active layer thicknesses for most of the grids display increasing linear trends, except for a small number of grids that were located in the west-central region of the permafrost area, which display negative linear trends. The grids with the shallowest

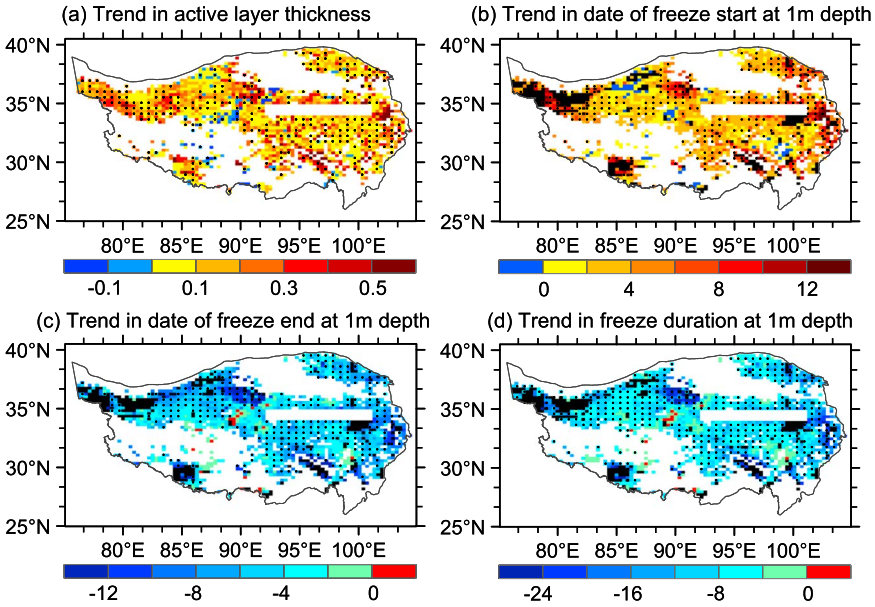

Figure 11. Trends in the (a) simulated active layer thickness (m/decade), (b) date of freeze start at 1 m depth (day/decade), (c) date of freeze end at 1 m depth (day/decade), and (d) freeze duration at 1 m depth (day/decade) for permafrost from 1981 to 2010. Similar to Figure 8, the data in the belt near 34.10°N to 35.04°N; 92.19°E to 100.93°E were removed. Black grids represent those areas where soil does not thaw to 1 m depth over the course of at least 1 year from 1981 to 2010. Areas with significance level exceeding 95% are denoted with dots.

current active layer thicknesses, e.g., in the northwestern corner of permafrost area, experienced smaller increases in their active layer thicknesses, with a range of approximately 0–0.10 m/decade. Over the entire permafrost area, the majority of trends in the active layer thickness ranged from 0 to 0.50 m/decade, the maximum trend was 0.70 m/decade locally, with an area-averaged value of 0.15 m/decade.

[31] *Oelke and Zhang* [2007] simulated a trend in the active layer thickness on the Tibetan Plateau of 0.14 m/decade for their northern subregion, 0.12 m/decade for the discontinuous permafrost area, and 0.07 m/decade for the sporadic permafrost area from 1980 to 2001. Despite the different research period and permafrost area, our result was similar to, but slightly larger than, that of *Oelke and Zhang* [2007]. Our

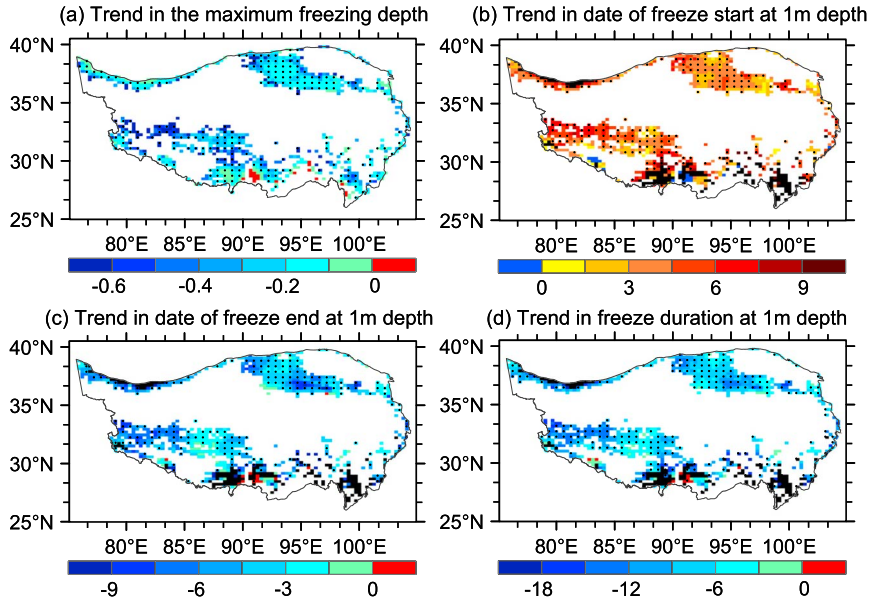

Figure 12. Trends in the (a) simulated maximum freezing depth (m/decade), (b) date of freeze start at 1 m depth (day/decade), (c) date of freeze end at 1 m depth (day/decade), and (d) freeze duration at 1 m depth (day/decade) for seasonally frozen ground from 1981 to 2010. Black grids represent those areas where soil does not freeze to 1 m depth over the course of at least 1 year from 1981 to 2010. Areas with significance level exceeding 95% are denoted with dots.

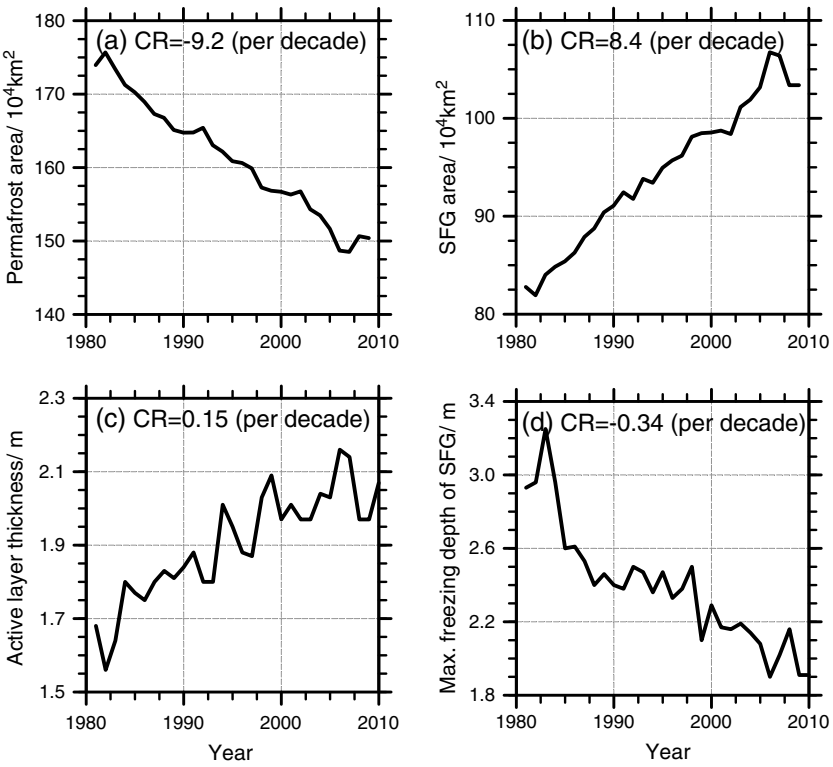

Figure 13. Time series of the (a) simulated near-surface permafrost area (including glaciers and lakes), (b) time series of the simulated seasonally frozen ground (SFG) area (including glaciers and lakes), (c) the area-mean time series of the simulated active layer thickness, averaged over the minimum permafrost area from 1981 to 2010, and (d) the area-mean time series of the simulated maximum freezing depth, averaged over the minimum seasonally frozen ground area from 1981 to 2010. CR denotes a change in rate.

results were also basically consistent with the magnitude of the trends in the active layer thicknesses (0.10–0.50 m/decade) from southern Alaska, northern Canada, and south-central Siberia [*Oelke et al*., 2004].

[32] The simulated date of freeze start at 1 m depth for almost all of the grids in the permafrost area displayed a delaying trend, except for a small number of grids that were scattered in the permafrost area. Most of the trends in the date of freeze start ranged from 0 to 12 days/decade for the entire permafrost area, with an area-averaged value of 3.8 days/decade. In contrast, the simulated date of freeze end at 1 m depth displayed an advancing trend for nearly all of the grids. There were also a few grids with delaying trends in the freeze end date. Most of the trends in the date of freeze end ranged from −12 to 0 days/decade for the whole permafrost area, with an area-averaged value of −5.9 days/decade. Both the delaying trend for the freeze start date and the advancing trend for the freeze end date resulted in shorter freeze durations, with a majority of the trends ranging from −24 to 0 and an area-averaged value of −9.7 days/decade.

[33] Figure 12 presents the spatial pattern of trends for the maximum freezing depth, the date of freeze start, the date of freeze end, and the freeze duration at a depth of 1 m for seasonally frozen ground from 1981 to 2010. Almost all of the grids experienced decreasing trends in the maximum freezing depth, except for a few grids that were located in the southern region of the seasonally frozen ground area. Basically, the grids with relatively shallow current maximum freezing depths, e.g., in the center of the seasonally frozen ground area, have smaller decreasing trends in maximum freezing depth, while the grids with relatively deep current maximum freezing depths, e.g., at the edge of the seasonally frozen ground area, have larger decreasing trends for maximum freezing depth. For the whole seasonally frozen ground area, most of the trends in the maximum freezing depth ranged from −0.60 to 0 m/decade, and the area-averaged trend was −0.34 m/decade. Similar to permafrost areas, the simulated date of freeze start, date of freeze end, and freeze duration at 1 m depth for the majority of the grids in the seasonally frozen ground area also experienced delaying, advancing, and shortening trends, respectively, except for a few grids that were located in the southern region of the seasonally frozen ground area. The majority of the trends ranged from 0 to 9 days/decade, from −9 to 0 days/decade, and from −18 to 0 days/decade, respectively, and their area-averaged trends were 4.0 m/decade, −4.6 m/decade, and −8.6 m/decade, respectively.

[34] Based on the daily Special Sensor Microwave/Imager (SSM/I) data, *Li et al*. [2012] reported that the date of freeze start for near-surface soil was delayed by 5 days/decade, the date of freeze end in the near-surface soil was advanced by 7 days/decade, and freeze duration for near-surface soil was shortened by 16.8 days/decade on the Tibetan Plateau from 1988 to 2007. By comparison, our simulated results indicated a delaying trend of approximately 3.9 days/decade (permafrost: 3.8 days/decade, seasonally frozen ground: 4.0 days/decade) in the date of freeze start at 1 m depth, an advancing trend of approximately

5.3 days/decade (permafrost: 5.9 days/decade, seasonally frozen ground: 4.6 days/decade) in the date of freeze end at 1 m depth, and a shortening trend of approximately 9.2 days/decade (permafrost: 9.7 days/decade, seasonally frozen ground: 8.6 days/decade) in the freeze duration at 1 m depth from 1981 to 2010. Apparently, the magnitude of our work was close to, but smaller than, that of *Li et al.* [2012]. The deviation between these two works might be partially due to the difference in two research periods and the difference in two soil depths. More reasons for the deviation require further evaluation in the future.

[35] The time series for the simulated permafrost area, seasonally frozen ground area, active layer thickness, and the maximum freezing depth are displayed in Figure 13. The time series of the permafrost area indicated a significant decreasing trend, with a rate of 9.20×10^4 km^2/decade from 1981 to 2010. This decreasing rate was somewhat larger than the rate of 7.60×10^4 km^2/decade during the same period that was reported by *Guo et al.* [2012], which results from the different atmospheric forcing data. This time series for the Plateau's permafrost area was consistent with that of the Northern Hemisphere permafrost area simulated by CCSM4 in the 1980s and in 1990s [*Lawrence et al.*, 2012].

[36] The loss of permafrost occurred at the edge, especially the southern edge of the simulated permafrost boundary. The losing permafrost was converted into seasonally frozen ground, thus resulting in the increase in the seasonally frozen ground area. The loss of the seasonally frozen ground occurred at the southern edge of the Tibetan Plateau, which was reflected in that it is converted into the unfrozen ground. Large loss in the permafrost and relatively slight increase in the unfrozen ground result in the time series of the seasonally frozen ground area basically having a pattern that was essentially opposite to that of the permafrost area, with a trend of 8.40×10^4 km^2/decade.

[37] The time series for the active layer thickness displayed an increasing trend, with evident interannual changes. It had a statistically significant correlation coefficient of 0.7 with the time series of active layer thicknesses that was reported by *Guo et al.* [2012]. The deviation between these two results was attributed to the different atmospheric forcing data that were used by these two studies. Interannual changes were also evident in the time series of the maximum freezing depth, which displayed a decreasing trend.

4. Discussion

[38] The physics-based simulation of frozen ground is especially difficult on the Tibetan Plateau due to the lack of high-resolution atmospheric forcing data and reliable frozen ground models. Consequently, a suite of new, high-resolution atmospheric forcing data and the CLM4 model has been developed and released [*He*, 2010; *Chen et al.*, 2011; *Lawrence et al.*, 2011]. Using CLM4, forced by this suite of high-resolution atmospheric forcing data, our work simulated the current frozen ground state and changes in the frozen ground during the recent decades on the Tibetan Plateau. The model simulated a current permafrost area of 151.50×10^4 km^2. This area was close to, but slightly larger than, the ranges of permafrost areas reported in previous studies that were based on different methods. These methods included a regional statistical survey, a historical data analysis, a digitized map, and some statistical-empirical models (Table 2). The large differences in research methods between the present work and previous research could be a primary cause of the deviation in the permafrost areas. Conversely, the current permafrost area in the present work is 29.30×10^4 km^2 larger than the result reported by *Guo et al.* [2012], despite the single difference of atmospheric forcing data between these two studies. This discrepancy indicates that the permafrost simulation is also very sensitive to the atmospheric forcing data. Because air temperature is a climatic factor that is closely related to the permafrost simulation, we further compared the air temperatures of the atmospheric forcing data used by these two studies (Figure 5). From 1981 to 2000, the area-mean HY air temperature was 0.17°C lower than the RegCM3 air temperature used in the work of *Guo et al.* [2012]. The lower air temperature of the HY data could be a primary cause of the larger permafrost area in the present work. The differences in the other forcing elements, e.g., precipitation (snowfall) and radiation, may also have resulted in the deviation of the permafrost area between these two studies to some extent.

[39] The present work also investigated permafrost change in response to climate warming on the Tibetan Plateau during 1981 to 2010. This warming consists of an area-mean rate of increase of 0.44°C/decade. As shown by Figure 4a, a large portion of the Plateau has experienced a significant warming trend. The increases in air temperature were more significant in the northern, central, and western regions of the Plateau. With this amplitude of increase in air temperature, the CLM4 simulated that the near-surface permafrost area could decrease by 9.20×10^4 km^2/decade, and the active layer thickness could increase by 0.15 m/decade. The results are close to, but larger than, the decreasing rate of 7.60×10^4 km^2/decade for permafrost areas and the increasing rate of 0.17 m/decade for active layer thicknesses during the same period that were reported by *Guo et al.* [2012]. The deviation between these two research results can be attributed to the difference in their atmospheric forcing data. In the present work, the time series and the increasing rates of HY air temperature agree well with those of the CN05 air temperature (Figure 5), which provided an assurance of the rationality of the simulated frozen ground changes in the present work.

[40] We evaluated the air temperature and precipitation of the atmospheric forcing data, which are thought to be closely related to the frozen ground simulation [*Lawrence et al.*, 2012; *Guo et al.*, 2012]. However, the other forcing elements, e.g., radiation and wind speed, did not obtain a systemic evaluation due to the lack of observed data. To fully clarify the biases in the atmospheric forcing data and their possible impacts on the simulated results, more observed data are needed in the future. In addition, the observed site data used to validate the simulated results are sparse. This sparseness resulted in a partial scale mismatch in the comparison between the simulated results and observations. Undoubtedly, this lack of data makes it difficult to more reasonably simulate frozen ground on the Tibetan Plateau. One solution for this problem is to establish denser observation sites in the future. Another solution is to further enhance the spatial resolution of the model. However, this may be challenging because a higher-resolution model also requires finer and more accurate surface, soil organic matter, and soil texture data sets.

[41] Similar to the work by *Guo et al*. [2012], the present study also encountered a belt of unchanging active layer thickness with the same area approximately 34.10°N to 35.04°N and 92.19°E to 100.93°E, which was related to the possible inaccuracy of the soil organic matter content in these locations. The simulated frozen ground parameters in this belt may be inaccurate and, thus, they were removed. In the other regions, e.g., the eastern region of the Plateau, the inaccuracies in the soil organic matter content may be small but could also cause the bias in the permafrost simulation to some extent. In addition, possible inaccuracies in the other surface and soil texture data sets were also notable for their contribution to the uncertainties in the simulation of frozen ground.

[42] Snow cover is crucial for permafrost simulation due to its insulating effect, which mediates thermal connection between the air and land surface, thus affecting the simulated soil thermal environments [*Yang et al*., 2008; *Koven et al*., 2012]. In this work, total precipitation was inputted as forcing data, and then the model used a formulation based on air temperature to determine the precipitation in solid and/or solid form. This may bring some biases in snowfall and the related uncertainties in permafrost simulation. Therefore, individual input of accurate solid and liquid precipitation or a sophisticated method of dividing solid and liquid precipitation in model would be helpful for permafrost simulation.

5. Summary

[43] The new, high-resolution forcing data used in this study were of a higher quality and also advantageous to the Plateau's frozen ground simulation; we found that the simulated soil temperature was closer to our observations when forced by higher resolution temporal and spatial data. Moreover, these forcing data also produced a more detailed frozen ground distribution map than the previous work.

[44] Simulated permafrost covered a total area of 151.50×10^4 km^2, which is close to, but slightly larger than, the ranges from previous studies. The simulated area-mean active layer thickness is 2.01 m. The model also yielded the area-mean date of freeze start, date of freeze end, and freeze duration at a depth of 1 m for permafrost of approximately the 296th day (23 October), the 174th day (23 June), and 254 days, respectively. For seasonally frozen ground, the model yielded area-mean maximum freezing depth, date of freeze start, date of freeze end, and freeze duration at a depth of 1 m of approximately 2.47 m, the 342nd day (8 December), the 112th day (22 April), and 124 days, respectively.

[45] The simulated results were validated by comparing them to the corresponding site observations. They appeared to be reasonable, considering the known issues (e.g., scale mismatch).

[46] From 1981 to 2010, the permafrost area decreased significantly at a rate of 9.20×10^4 km^2/decade. Meanwhile, the active layer thickness increased at a rate of 0.15 m/decade. At 1 m depth of the entire frozen ground area, the model generated a delaying trend in the date of freeze start by a rate of approximately 3.9 days/decade and an advancing trend in the date of freeze end by a rate of approximately 5.3 days/decade. The delaying date of freeze start that was associated with the advancing date of freeze end resulted in a shorter freeze duration of approximately 9.2 days/decade.

[47] These results give detailed permafrost and seasonally frozen ground states as well as their changes during the recent decades. They will be useful for studying frozen ground's response to climate change and frozen ground engineering stabilization. Further discussions showed this study's uncertainties were primarily attributed to possible inaccuracies in the soil organic matter content and even in the other surface and soil texture data sets. Additional observed data and further enhancement of the spatial resolution of the model will improve the simulation of frozen ground on the Tibetan Plateau in the future. Continued work will investigate the near-surface soil freeze/thaw conditions and diurnal freeze/thaw cycles of the ground surface on the Tibetan Plateau and their changes in recent decades.

[48] **Acknowledgments.** This research was jointly supported by the National Natural Science Foundation of China under Grants (41130103 and 41210007). Thanks are due to Kun Yang and Jie He for providing the high-resolution atmospheric forcing data sets. Thanks are also due to Meixue Yang for providing partial soil temperature observations for the validation of the simulated results. We are indebted to three reviewers for helpful comments and criticisms of the initial draft of this paper.

References

Alexeev, V. A., D. J. Nicolsky, V. E. Romanovsky, and D. M. Lawrence (2007), An evaluation of deep soil configurations in the CLM3 for improved representation of permafrost, *Geophys. Res. Lett.*, *34*, L09502, doi:10.1029/2007GL029536.

Burn, C. R., and F. E. Nelson (2006), Comment on "A projection of severe near-surface permafrost degradation during the 21st century" by David M. Lawrence and Andrew G. Slater, *Geophys. Res. Lett.*, *33*, L21503. doi:10.1029/2006GL027077.

Chen, Y., K. Yang, J. He, J. Qin, J. Shi, J. Du, and Q. He (2011), Improving land surface temperature modeling for dry land of China, *J. Geophys. Res.*, *116*, D20104, doi:10.1029/2011JD015921.

Cheng, G., and T. Wu (2007), Responses of permafrost to climate change and their environmental significance, Qinghai-Tibet Plateau, *J. Geophys. Res.*, *112*, F02S03, doi:10.1029/2006JF000631.

Crawford, T. M., and C. E. Duchon (1999), An improved parameterization for estimating effective atmospheric emissivity for use in calculating daytime downward long-wave radiation, *J. Appl. Meteorol.*, *38*, 474–480.

Delisle, G. (2007), Near-surface permafrost degradation: How severe during the 21st century?, *Geophys. Res. Lett.*, *34*, L09503, doi:10.1029/2007GL029323.

Gao, X. J., Y. Shi, D. F. Zhang, and F. Giorgi (2012), Climate change in China in the 21st century as simulated by a high resolution regional climate model, *Chin. Sci. Bull.*, *57*, 1188–1195, doi:10.1007/s11434-011-4935-8.

Guo, D. L., and H. J. Wang (2011), The significant climate warming in the northern Tibetan Plateau and its possible causes, *Int. J. Climatol.*, *32*, 1775–1781, doi:10.1002/joc.2388.

Guo, D. L., M. X. Yang, and H. J. Wang (2011a), Characteristics of land surface heat and water exchange under different soil freeze/thaw conditions over the central Tibetan Plateau, *Hydrol. Process.*, *25*, 2531–2541, doi:10.1002/hyp.8025.

Guo, D. L., M. X. Yang, and H. J. Wang (2011b), Sensible and latent heat flux response to diurnal variation in soil surface temperature and moisture under different freeze/thaw soil conditions in the seasonal frozen soil region of the central Tibetan Plateau, *Environ. Earth Sci.*, *63*, 97–107, doi:10.1007/s12665-010-0672-6.

Guo, D. L., H. J. Wang, and D. Li (2012), A projection of permafrost degradation on the Tibetan Plateau during the 21st century, *J. Geophys. Res.*, *117*, D05106, doi:10.1029/2011JD016545.

He, J. (2010), Development of a surface meteorological dataset of China with high temporal and spatial resolution [in Chinese], Master Dissertation, Institute of Tibetan Plateau Research, Chinese Academy of Science.

Huffman, G. J., R. F. Adler, D. T. Bolvin, G. Gu, E. J. Nelkin, K. P. Bowman, Y. Hong, E. F. Stocker, and D. B. Wolff (2007), The TRMM multi-satellite precipitation analysis (TMPA): Quasi-global, multi-year, combined-sensor precipitation estimates at fine scales, *J. Hydrometeorol.*, *8*, 38–55, doi:10.1175/JHM560.1.

Jin, H. J., X. L. Chang, and S. L. Wang (2007), Evolution of permafrost on the Qinghai-Xizang (Tibet) Plateau since the end of the late Pleistocene, *J. Geophys. Res.*, *112*, F02S09, doi:10.1029/2006JF000521.

Ju, L. X., H. J. Wang, and D. B. Jiang (2007), Simulation of the Last Glacial Maximum climate over East Asia with a regional climate model nested in a general circulation model, *Palaeogeogr. Palaeoclimatol. Palaeoecol.*, *248*, 376–390, doi:10.1016/j.palaeo.2006.12.012.

Koven, C. D., W. J. Riley, and A. Stern (2012), Analysis of permafrost thermal dynamics and response to climate change in the CMIP5 Earth System Models, *J. Clim.*, doi:10.1175/JCLI-D-12-00228.1.

Lawrence, D. M., and A. G. Slater (2005), A projection of severe near-surface permafrost degradation during the 21st century, *Geophys. Res. Lett.*, *32*, L24401, doi:10.1029/2005GL025080.

Lawrence, D. M., and A. G. Slater (2006), Reply to comment by C.R. Burn and F.E. Nelson on "A projection of near-surface permafrost degradation during the 21st century", *Geophys. Res. Lett.*, *33*, L21504, doi:10.1029/2006GL027955.

Lawrence, D. M., and A. G. Slater (2008), Incorporating organic soil into a global climate model, *Clim. Dyn.*, *30*, doi:10.1007/s00382-007-0278-1.

Lawrence, D. M., et al. (2011), Parameterization improvements and functional and structural advances in version 4 of the Community Land Model, *J. Adv. Model. Earth Syst.*, *3*, doi:10.1029/2011MS000045.

Lawrence, D. M., A. G. Slater, and S. C. Swenson (2012), Simulation of present-day and future permafrost and seasonally frozen ground conditions in CCSM4, *J. Clim.*, *25*, 2207–2225.

Li, S., and G. Cheng (1996), *Map of permafrost distribution on the Qinghai-Xizang (Tibetan) Plateau (1:3,000,000) [in Chinese]*, Gansu Cultural Press, Lanzhou.

Li, X., and G. Cheng (1999), A GIS aided response model of high altitude permafrost to global change, *Sci. China*, *42*, 72–79.

Li, X., J. Rui, X. Pan, T. Zhang, and J. Guo (2012), Changes in the near-surface soil freeze–thaw cycle on the Qinghai-Tibetan Plateau, *Int. J. Appl. Earth Observ. Geoinf.*, *17*, 33–42, doi:10.1016/j.jag.2011.12.002.

Liu, X., and B. Chen (2000), Climatic warming in the Tibetan Plateau during recent decades, *Int. J. Climatol.*, *20*, 1729–1742.

Nan, Z. (2003), Study of the characteristics of permafrost distribution on the Qinghai-Tibet Plateau and construction of digital roadbed of the Qinghai-Tibet railway [in Chinese], PhD Dissertation, Cold and Arid Regions Environmental and Engineering Research Institute, Chinese Academy of Sciences.

Nelson, F. (2003), (Un)frozen in time, *Science*, *299*, 1673–1675.

Nelson, F., O. Anisimov, and N. Shiklomanov (2001), Subsidence risk from thawing permafrost, *Nature*, *410*, 889–890.

Nicolsky, D. J., V. E. Romanovsky, V. A. Alexeev, and D. M. Lawrence (2007), Improved modeling of permafrost dynamics in a GCM land surface scheme, *Geophys. Res. Lett.*, *34*, L08501, doi:10.1029/ 2007GL029525.

Niu, G. Y., and Z. L. Yang (2006), Effects of frozen soil on snowmelt runoff and soil water storage at a continental scale, *J. Hydrometeorol.*, *7*, 937–952, doi:10.1175/JHM538.1.

Oelke, C., and T. Zhang (2007), Modeling the active-layer depth over the Tibetan Plateau, *Arctic Antarct. Alpine Res.*, *39*, 714–722.

Oelke, C., T. Zhang, and M. C. Serreze (2004), Modeling evidence for recent warming of the Arctic soil thermal regime, *Geophys. Res. Lett.*, *31*, L07208, doi:10.1029/2003GL019300.

Oleson, K., et al. (2010), Technical description of version 4.0 of the Community Land Model (CLM), NCAR Technical Note NCAR/TN-478+STR, National Center for Atmospheric Research, Boulder, CO, 266 pp.

Pinker, R. T., and I. Laszlo (1992), Modeling surface solar irradiance for satellite applications on a global scale, *J. Appl. Meteorol.*, *31*, 194–211.

Qiu, G., and G. Cheng (1995), Permafrost in China: Past and present, *Perma. Perigl. Proc.*, *6*, 3–14.

Ran, Y. H., X. Li, G. D. Cheng, T. J. Zhang, Q. B. Wu, H. J. Jin, and R. Jin (2012), Distribution of permafrost in China: An overview of existing permafrost maps, *Perma. Perigl. Proc.*, *23*, 322–333, doi:10.1002/ppp.1756.

Schuur, E., J. Vogel, K. Crummer, H. Lee, J. Sickman, and T. Osterkamp (2009), The effect of permafrost thaw on old carbon release and net carbon exchange from tundra, *Nature*, *459*, 556–559.

Sheffield, J., G. Goteti, and E. F. Wood (2006), Development of a 50-year high-resolution global dataset of meteorological forcings for land surface modeling, *J. Clim.*, *19*, 3088–3111, doi:10.1175/JCLI3790.1.

Sun, J. Q., H. J. Wang, W. Yuan, and H. P. Chen (2010), Spatial-temporal features of intense snowfall events in China and their possible change, *J. Geophys. Res.*, *115*, D16110, doi:10.1029/2009JD013541.

Wang, X. L. L., and V. R. Swail (2001), Changes of extreme wave heights in Northern Hemisphere oceans and related atmospheric circulation regimes, *J. Clim.*, *14*, 2204–2221.

Wang, A., and X. Zeng (2011), Sensitivities of terrestrial water cycle simulations to the variations of precipitation and air temperature in China, *J. Geophys. Res.*, *116*, D02107, doi:10.1029/2010JD014659.

Wang, A., and X. Zeng (2012), Evaluation of multireanalysis products with in situ observations over the Tibetan Plateau, *J. Geophys. Res.*, *117*, D05102, doi:10.1029/2011JD016553.

Wang, S., H. Jin, S. Li, and L. Zhao (2000), Permafrost degradation on the Qinghai-Tibet Plateau and its environmental impacts, *Perma. Perigl. Proc.*, *11*, 43–53.

Wei, F. (2007), *Statistical Diagnosis and Prediction Technology of the Modern Climate [in Chinese]*, 296 pp., Beijing: China Meteorological Press.

Wu, Q., and T. Zhang (2008), Recent permafrost warming on the Qinghai-Tibetan Plateau, *J. Geophys. Res.*, *113*, D13108, doi:10.1029/2007JD009539.

Wu, Q., and T. Zhang (2010), Changes in active layer thickness over the Qinghai-Tibetan Plateau from 1995 to 2007, *J. Geophys. Res.*, *115*, D09107, doi:10.1029/2009JD012974.

Wu, Q., T. Zhang, and Y. Liu (2010), Permafrost temperatures and thickness on the Qinghai-Tibet Plateau, *Glob. Planet. Change*, *72*, 32–38.

Xu, Y., X. Gao, Y. Shen, C. Xu, Y. Shi, and F. Giorgi (2009), A daily temperature dataset over China and its application in validating a RCM simulation, *Adv. Atmos. Sci.*, *26*, 763–772.

Yang, K., T. Koike, and B. Ye (2006), Improving estimation of hourly, daily, and monthly downward shortwave radiation by importing global datasets, *Agric. Forest Meteorol.*, *137*, 43–55, doi:10.1016/j.agrformet. 2006.02.001.

Yang, M. X., T. D. Yao, and X. H. Gou (2003), The soil moisture distribution, thawing freezing processes and their effects on the seasonal transition on the Qinghai-Xizang (Tibetan) plateau, *J. Asian Earth Sci.*, *21*, 457–465.

Yang, M. X., T. D. Yao, F. Nelson, N. Shiklomanov, D. L. Guo, and C. Wang (2008), Snow cover and depth of freeze-thaw on the Tibetan Plateau: A case study from 1997 to 1998, *Phys. Geogr.*, *29*, 208–221, doi:10.2747/0272-3646.29.3.208.

Yang, M. X., F. E. Nelson, N. I. Shiklomanov, D. L. Guo, and G. Wan (2010), Permafrost degradation and its environmental effects on the Tibetan Plateau: A review of recent research, *Earth Sci. Rev.*, *103*, 31–44.

Yatagai, A., O. Arakawa, K. Kamiguchi, H. Kawamoto, M. I. Nodzu, and A. Hamada, (2009), A 44-year daily gridded precipitation dataset for Asia based on a dense network of rain gauges, *SOLA*, *5*, 137–140, doi:10.2151/sola.2009-035.

Yi, S., M. K. Woo, and M. A. Arain (2007), Impacts of peat and vegetation on permafrost degradation under climate warming, *Geophys. Res. Lett.*, *34*, L16504, doi:10.1029/2007GL030550.

Zhao, L. (2004), The freezing-thawing processes of active layer and changes of seasonally frozen ground on the Tibetan Plateau [in Chinese], PhD Dissertation, Cold and Arid Regions Environmental and Engineering Research Institute, Chinese Academy of Science.

Zhou, Y., and D. Guo (1983), Some features of permafrost in China, Proceedings of the 4th International Conference on Permafrost, National Academy Press, Washington DC, volume l, pp. 1496–1501.

Zimov, S., E. Schuur, and F. Chapin III (2006), Permafrost and the global carbon budget, *Science*, *312*, 1612–1613.